3.1 MHD

3.1.1 Optimizing Macroscopic Stability in the Spherical Torus

Plasma stability at high plasma pressure is required for economically attractive operation of a thermonuclear fusion reactor based on magnetic confinement. For nearly all magnetic confinement concepts, engineering constraints limit the maximum magnetic field that can be applied to contain the plasma, so an important figure of merit for magnetic fusion devices is the plasma beta $\beta \equiv 2\mu_0 p/B^2$ where p is the plasma pressure and B is the magnetic field within the plasma. For tokamak plasmas, the plasma pressure can vary significantly across the plasma cross-section and the applied toroidal field dominates the total field and varies comparatively little within the plasma. Thus, a commonly used tokamak figure of merit is the toroidal beta $\beta_T \equiv 2\mu_0\langle p\rangle/B_{T0}^2$ where $\langle p\rangle$ is the volume-averaged pressure and B_{T0} is the vacuum toroidal field at the plasma geometric center. Experiments to date have shown that ideal magnetohydrodynamic (MHD) stability theory provides an accurate description of the maximum stable beta for tokamak plasmas. It is expected that this should also be true for spherical torus [1] (ST) plasmas. However, the high beta and low aspect ratio geometry of the ST can lead to significant alteration of stability physics in several important respects. For instance, the elevated safety factor and large edge magnetic shear, high core rotation and rotational shear, and comparatively low Alfvén speed and associated enhanced drive for fast-ion instabilities are each unique characteristics of the ST, which must be independently evaluated for their impact on stability. It is also expected this evaluation will benefit significantly from proposed "similarity" experiments with standard aspect ratio tokamaks (DIII-D) and other ST devices (MAST), which will attempt to determine the role of aspect ratio in the physics of several MHD modes, including resistive wall modes, neoclassical tearing modes, and Alfvén eigenmodes.

For the advanced tokamak (AT) and ST concepts to lead to efficient steady-state reactors, high beta alone is insufficient. In particular, most reactor design studies have shown that it is important to have a large fraction of the plasma current be self-generated through the neoclassical bootstrap effect to minimize power requirements for auxiliary systems. Plasma current profiles in largely bootstrap current driven equilibria are generally broad with low plasma internal inductance, l_i. Tokamak experience has shown that another important beta parameter, the normalized beta $\beta_N \equiv \beta_T(\%)aB_0/I_P(MA)$ may decrease with

decreasing l_i [2,3,4] in the absence of wall stabilization. Since $\beta_T \propto \beta_N{}^2$ when the bootstrap fraction is held fixed, it is critical to test such scaling in both the AT and ST.

The potential incompatibility between high β and efficient self-sustainment has motivated several theoretical investigations of the stabilization of highly bootstrapped AT [5,6] and ST [7] plasmas. Significant experimental progress has already been made in removing this incompatibility in advanced tokamak plasmas by combining conducting structure (wall stabilization) with plasma rotation [8,9] and feedback systems [10] to achieve values of β_T significantly above the level possible without stabilizing systems [11]. Applying this experience and understanding to the ST is particularly important, since design studies [12] indicate that a self-sustained ST reactor would simultaneously require β_N values well above and l_i values well below those achieved in present advanced tokamaks.

The programmatic focus of MHD studies in NSTX in the coming five years will be to optimize ST plasma stability in discharges lasting significantly longer than a current diffusion time with beta values significantly above the no-wall stability limit with a large fraction of the plasma current being self-generated. In the near term, optimization of plasma shape and profiles, error-field correction, and feedback suppression of the resistive wall mode are viewed as capabilities most likely to aid in the achievement of the above goals. Neoclassical tearing modes, fast-ion-driven MHD, and edge-localized modes (ELMs) have already been observed to often have a deleterious impact on performance. It is also expected that significant progress in the understanding and control of these modes will be made as improved diagnostics and additional heating and current profile control tools become available.

3.1.2 Overview of Research Plans for FY2004-2008

Much of NSTX research over the next five to ten years is tightly linked to the IPPA ST ten-year goal of achieving long-pulse operation at high performance. Sub-sections of the IPPA five and ten-year ST operational goals and the IPPA science goal are listed below for reference. The underlined and italicized segments of the goals pertain most directly to MHD research on NSTX.

IPPA — ST Five-year goal: Make a preliminary assessment of the attractiveness of the ST regarding confinement, *stability, and high-beta operations*, and non-inductive operations (to be achieved early in the 2004-2008 time frame).

IPPA — ST Ten-year goal: Assess the attractiveness of extrapolable, *long-pulse operation* of the spherical torus for time scales much greater than the current penetration time scales (to be achieved in the 2009 timeframe).

IPPA science goal 1: Advance the *fundamental understanding of plasmas*... and enhance predictive capabilities through *comparison of experiments, theory, and simulation*.

The IPPA five-year ST goal as it relates to MHD effectively calls for a preliminary assessment of the MHD stability limits of NSTX and a further assessment as to whether these achieved limits are attractive. Ultimately, this attractiveness must be judged by whether or not the beta values obtainable in long-pulse and with high bootstrap fraction are relevant to future reactor-scale devices such as a volume neutron source, a component test facility, or even a demonstration reactor.

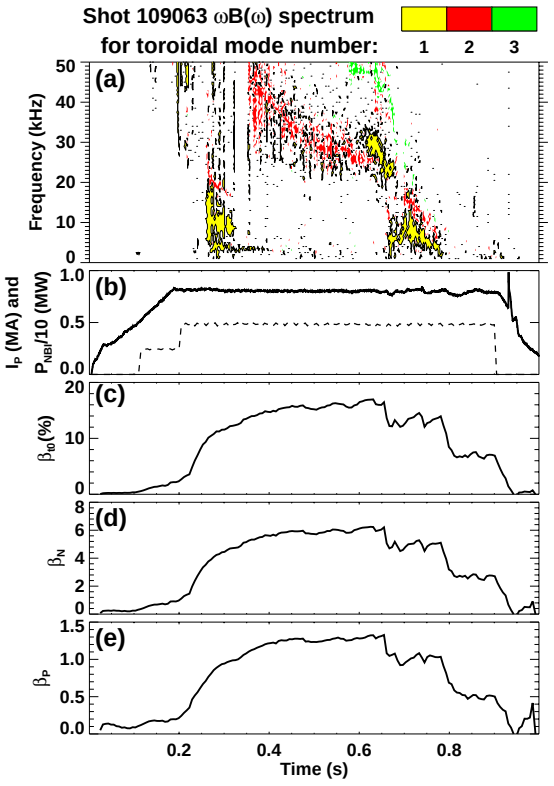

Figure 3.1.1 - Mirnov frequency and toroidal mode number spectrogram and β parameters for a long-pulse NSTX discharge with $\beta_N \approx 6$.

The rapid progress of the NSTX team toward making such assessments becomes more obvious when one considers that the MHD group is already beginning to study stability physics related to the IPPA ST ten-year goal – extrapolative long-pulse operation. In particular, recent experiments within the MHD and Integrated Scenario Development (ISD) experimental task groups have obtained discharges with total pulse length just over 1 second, 700ms I_P = 800kA flat-top duration, and β_N=6 and

β_T=16% held in near steady-state for at least one current relaxation time (τ_{CR} = 200-250ms). The MHD modes present in this discharge and other β parameters of interest are shown in Figure 3.1.1. Of particular interest in these long-pulse high-β_N shots are the largely internal disruptions in stored energy whose cause is not yet fully understood. The most likely explanations given the present understanding are: 1) that the q-profile is evolving to an unstable state, possibly a reverse-shear q profile, which destabilizes double tearing modes at large minor radius, or 2) the plasma is reaching the ideal with-wall beta limit and is undergoing a disruption with very weak external component. Without MSE, it is not yet possible to infer if double tearing modes are the cause of these disruptions. It is noteworthy that these long-pulse discharges can be run quiescently with β_N up to 5.8, while attempting to push to higher $\beta_N > 6$ often leads to internal disruptions with a prompt loss of 5-20% of the total stored energy at high $B_T > 4.5$kG. Rapidly growing (τ=200-500μs) n=1 precursors are observed just prior to these collapses at frequencies (15-25kHz) well above the edge-rotation frequency, so it is likely that these modes are either ideally driven or are driven by fast particles rather than by near-edge tearing modes, although strongly driven core tearing modes cannot be definitively ruled out.

Previous theoretical calculations have shown that ideal-wall beta limits with $\beta_N > 8$ are possible in NSTX with optimized profiles. In particular, a broad total pressure peaking factor < 2.5 is highly advantageous for strong coupling to the stabilizing passive plates. For reference, the thermal pressure peaking factor in NSTX H-modes is typically near 2. In addition, a q profile with $q(0) > 2$ with either monotonic or weakly reversed shear has been shown to improve low toroidal mode number stability by eliminating low-order mode rational surfaces while simultaneously aligning the total current profile with the off-axis bootstrap current resulting from the broad thermal pressure profile. Important elements in achieving very high β limits in self-sustaining operation are strongly linked to the transport properties of NSTX plasmas. Just a few examples of this transport/MHD synergy include: 1) understanding the role of plasma shape and divertor geometry in thermal confinement, particle confinement, impurity control, and pressure peaking, 2) understanding the role of saturated NTMs in confinement degradation, and 3) understanding the role of fast-ion MHD in the diffusion and loss of NBI fast-ions and its associated impact on the pressure, rotation, heating, and current-drive profiles from NBI.

3.1.3 Macroscopic Stability Results and Plans by Topical Area

The issues discussed above in the MHD programmatic overview highlight the need for improved diagnostics and control tools in NSTX to accurately assess the attractiveness of the ST concept in the near-term and in the five to ten-year time frame. The following subsections provide a list of topical areas and a fiscal year timeline for achieving the required physics, diagnostic, and control tools in each area.

Recent macroscopic stability improvements

NSTX has made significant progress during the past year in reaching high beta under a wide range of operating conditions. As seen in Figure 3.1.2, normalized beta values of $\beta_N > 6$ were achieved during the FY2002 run (shown in red) for normalized currents in the range of 2.5 to 5MA/mT. By operating at high normalized current $I_P/aB_{T0} > 6$ with I_P=1.2MA and B_{T0}=0.3 Tesla, toroidal beta values as high as β_T=35% with $\beta_N > 5$ were achieved. As seen in the figure, both β_T and β_N values have increased by as much as a factor of 2 relative to operation in FY2001.

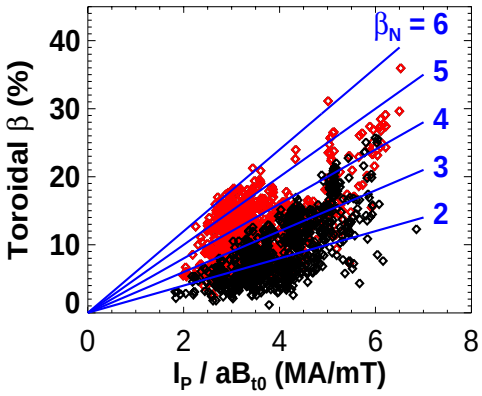

Figure 3.1.2 – Toroidal β(%) vs. I/aB

Future steady-state ST devices will need to rely heavily on the neoclassical bootstrap current to generate much of the toroidal plasma current, so achieving high values of poloidal beta is essential to the ST concept. Figure 3.1.3 shows that NSTX has more than doubled its poloidal beta values in the last year and has achieved $\varepsilon\beta_P \approx 0.8$–1 for cylindrical kink safety factor q^* = 2.5–3.5 where $q^* \equiv 20\varepsilon\beta_P/\beta_N$. For reference, NSTX target equilibria with β_T=40%, $\beta_N > 8$, and f_{BS} = 50–80% are indicated by the green region in Figure 3.1.3 and have $\varepsilon\beta_P$ values similar to those achieved experimentally. As seen in the same figure, a roughly 35% increase in

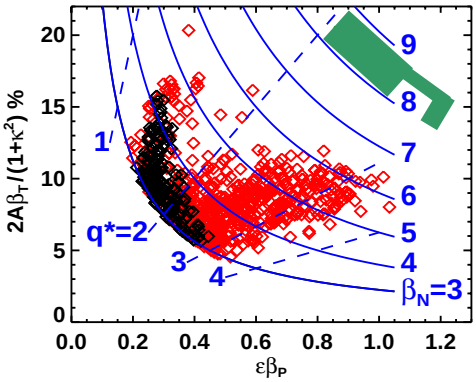

*Figure 3.1.3 – Poloidal and normalized β vs. q**

experimental β_N would be needed to access β_N values > 8 typical of a fully self-sustaining ST-based reactor or a high-bootstrap-fraction steady-state component test facility (CTF).

Several operational and facility improvements aided in achieving the high stability parameters shown above. These improvements include more optimal plasma profiles from reliable H-mode access, improved plasma shaping, error-field reduction, and elevated plasma safety factor. The influence of these improvements is discussed below.

Influence of profiles and shape on global stability – Results

Plasma profile effects

At the beginning of the FY2002 run campaign, NSTX gained the capability of high-temperature (350°C) bake-out of its graphite plasma facing components. This led to comparatively easy access to the H-mode and significantly broader pressure profiles that are predicted to improve stability in various NSTX operating regimes. These improvements are synergistic, as H-mode operation prior to error-field reduction (discussed later in this section) was often degraded by the excitation of 2/1 tearing modes, which often slowed, locked, and disrupted the plasma [13]. Consistent with theoretical expectations discussed above, Figure 3.1.4 shows a clear trend of increasing β_N with decreasing pressure peaking factor $p(0)/\langle p\rangle$ in NSTX. In this figure, the pressure peaking is determined as a best fit to external poloidal magnetic signals, the measured diamagnetic flux, and a scaled electron pressure profile as a loose fitting constraint. This peaking factor is typically well correlated to the peaking factor of the thermal pressure component of NSTX plasmas.

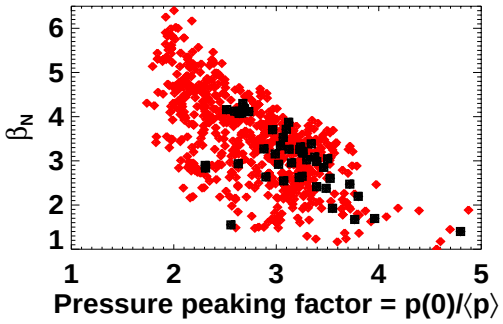

Figure 3.1.4 - β_N versus pressure peaking

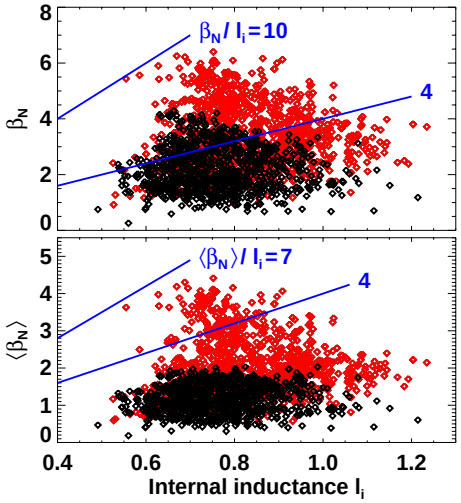

Figure 3.1.5- β_N versus internal inductance

Broad current profiles from the large off-axis bootstrap current density resulting from these broad pressure profiles are also predicted to improve wall stabilized beta limits by removing low-order mode-rational surfaces. Given the research goal of accessing very low l_i regimes at high β_N, an important question in NSTX stability research is the beta limit scaling with internal inductance. As stated above, some higher aspect ratio experiments have shown that the no-wall normalized beta limit obeys $\beta_N \approx 4 \times l_i$ [4]. Figure 3.1.5 shows that this empirical limit has been exceeded by a factor of 2.5 at intermediate values of l_i = 0.6, and shows that even $\langle \beta_N \rangle \equiv \langle \beta \rangle a B_{T0} / I_P$ where $\langle \beta \rangle \equiv 2\mu_0 \langle p \rangle / \langle B^2 \rangle$ exceeds $4 \times l_i$ by as much as a factor of 1.7. Perhaps more important than the high β_N / l_i ratio is the trend of increasing β_N with decreasing l_i evident in the figures. Testing this trend at lower l_i and assessing the influence of wall stabilization are important research topics, and future experiments will develop lower l_i discharges to investigate beta limits at l_i values approaching those of the NSTX design target.

Influence of plasma shape

Increased plasma shaping is well known to improve tokamak ideal MHD stability, and NSTX is now able to routinely access significantly higher elongation and triangularity. As seen by the black symbols in Figure 3.1.6, there was previously little advantage to operating with elongation much above 1.8 in most discharges. Stability analysis for L-mode discharges obtained prior to machine improvements found that n=1 internal pressure-driven kink mode stability is degraded for elongation values above 1.8 when the pressure profile is sufficiently peaked — consistent with the data shown in Figure 3.1.6. For the data following machine improvements shown in red, the broader pressure profile reduces the internal kink drive and excites a more global n=1 mode, which is more sensitive to boundary shaping and the influence of wall stabilization. Importantly, NSTX data now shows a trend of increasing β_N with increasing elongation up to at least κ = 2.1. The NSTX vertical control system is presently being upgraded to allow more routine access to even higher elongation to further test this trend.

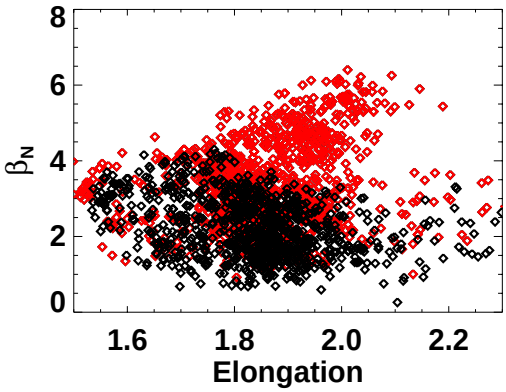

Figure 3.1.6 - β_N versus boundary elongation

As seen in Figure 3.1.7, NSTX also now more routinely operates at higher triangularity up to $\delta = 0.8$. Figure 3.1.7a shows that there is a relatively weak dependence of β_N on triangularity for $\delta > 0.4$, but as seen in Figure 3.1.7b, the highest β_T values have been achieved at the highest triangularity. Thus, the increase in β_T is a result of the ability to operate at higher normalized current presumably due to the increased edge safety factor and shear at high δ. Figure 3.1.7a also shows that β_N values have increased for all triangularity — consistent with the finding that much of the improved stability in NSTX has come from decreased pressure profile peaking.

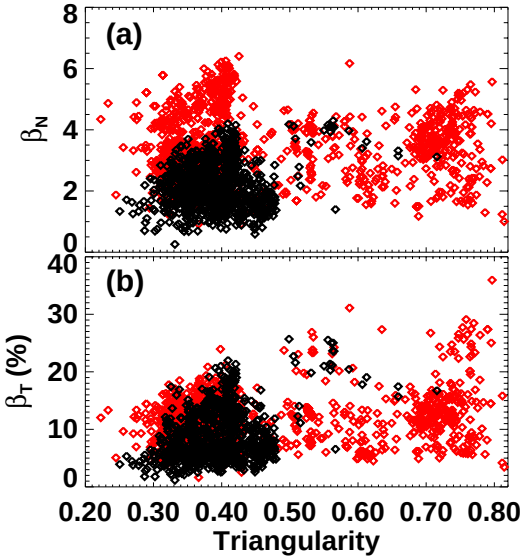

Figure 3.1.7 - β_N versus boundary triangularity

Influence of profiles and shape on global stability - Plans

Goal: *Measure and control the discharge shape and profiles to optimize stability and maximize the pulse duration at high performance.*

FY2003-04 Utilize isoflux control algorithm of real-time EFIT (rtEFIT) to improve boundary shape control during shot. Increase elongation and triangularity of lower single null discharges and/or elongation of highly triangular double null discharges to assess changes in normalized stability limits. Find optimum shape for highest global stability limit compatible with long-pulse requirement of tolerable ELMs in H-mode phase. Perform ramp-rate scans to determine fastest ramp-rate compatible with long-pulse. Assess confinement and pressure peaking as a function of discharge shape. Generate time evolving ideal stability analysis between shots to have immediate knowledge of the beta margin reached above the no-wall limit, and to generate significant statistics of such results.

FY2004-05 Utilizing MSE constrained reconstructions early during discharge ramp-up, use early heating and/or current drive from HHFW and/or NBI to slow current penetration. Optimize heating programming to elevate q profile above 2 with MHD-stable profile if present operating scenarios are not already doing this. Assess which MHD instabilities ameliorate the benefits of early heating and correlate with q profile dynamics. Assess normalized beta limits as a function of controllably low internal inductance. Experimentally access the second stability region to high-n ballooning modes in the ST by exploiting the synergistic stabilizing effects of low aspect ratio and high central safety factor. Determine the effect of finite Larmor radius (FLR), toroidal shear-flow, and other potential stabilization mechanisms of high-n modes in ST geometry by attempting to significantly violate the Mercier and high-n limits.

FY2004-06 Characterize dynamic evolution of equilibrium and compare to Tokamak Simulation Code (TSC) predictions to benchmark TSC resistivity, transport, heating, and current-drive models. Use physics knowledge gained to improve TSC as needed and to design controllers for heating and current-drive actuators, and to predict performance in future ST devices. Assess computationally MHD stability properties of promising scenarios identified with TSC.

FY2006-08 Utilize split PF1A coils to increase elongation up to 2.5 in low internal inductance plasmas. Utilize MSE-constrained rtEFITs to measure current profile in real-time. Use Plasma Control System (PCS) control of EBW and HHFW to heat and drive current to achieve desired current profile for optimized stability. Combine high κ operation with optimized NBI and RF current drive and investigate β-limiting instabilities in equilibria approaching the NSTX design target of $\beta_T = 40\%$ with $f_{BS} = 50\text{-}80\%$.

FY03-future Work to develop real-time predictive capability for stability. Consider neural network and other methods such as MHD spectroscopy. Implement PCS control of NBI, HHFW, and EBW to allow real-time feedback control of plasma beta. Use in conjunction with real-time stability information to operate just below relevant MHD stability limits.

Error fields and locked modes — Results and Status

Resonant error fields resulting from loss of axi-symmetry due to coil misalignments and other construction imperfections are well known to potentially lead to tokamak performance degradation [14,15,16]. This process appears to be particularly important near and above the ideal no-wall limit [11] where error-field amplification can lead to strong rotation damping and possible destabilization of the resistive wall mode (RWM) in advanced operating regimes. Early in the commissioning and calibration of the NSTX locked-mode detectors it became apparent that a 3–4cm effective shift of the lower PF5 vertical field coil was generating predominantly n=1 error-field over much of the NSTX plasma volume. The coil was subsequently shifted and re-shaped to minimize the n=1 error-field component. Measurements of the corrected coil shape indicate that the n=1 radial error-field strength from the PF5 coil has been reduced by at least an order of magnitude from roughly 12 Gauss at the outboard mid-plane to less than 1 Gauss. With regard to the resonant error field, the corresponding m/n = 2/1 vacuum island widths are computed to have been reduced from approximately 4cm to 0.7cm. This error-field reduction led immediately to improved performance — most noticeably in the locking behavior of ohmic discharges and beam-heated H-mode discharges. Figure 3.1.8 illustrates that prior to error field reduction (black curves) ohmic discharges routinely exhibited minor disruptions in plasma current and major disruptions in plasma density during the I_P flattop phase. In contrast, the red curves in Figure 3.1.8 show that following error-field reduction there is no locking behavior evident until the solenoid current limit is reached (near t=290ms) and strong negative loop voltage is applied that disrupts the plasma.

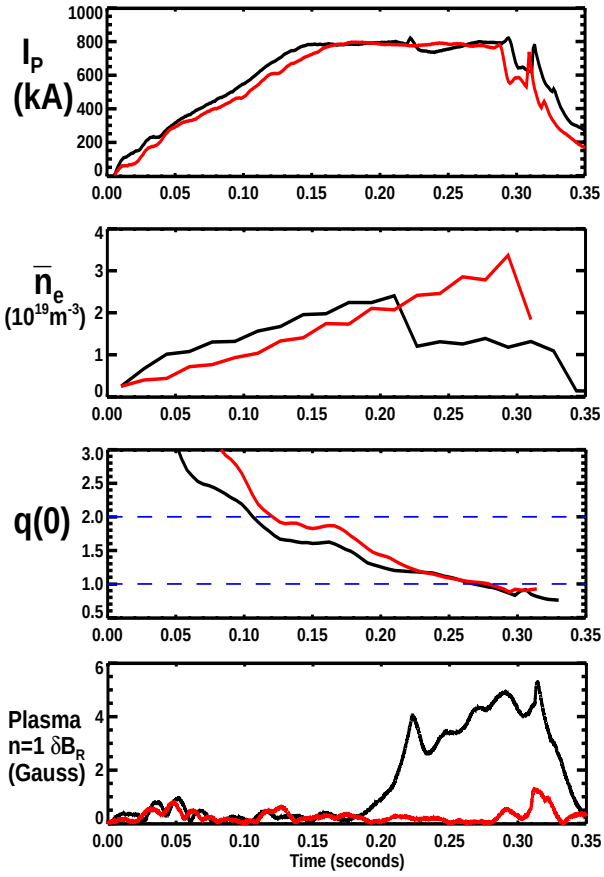

Figure 3.1.8 - Locked mode signatures before (black) and after error (red) field correction

While significant error-field reduction was achieved through re-shaping of the PF5 coil, other sources of error field may still be present in NSTX. Such sources include asymmetric mounting of the passive plates and all other PF coils on NSTX whose detailed shapes have not been measured due to access restrictions. As mentioned above, error fields can lead to error-field amplification of the resistive wall mode, rotation decay, and mode locking. Indeed, at sufficiently low density in NSTX, ohmic locked modes are still observed to lock at preferred toroidal locations — albeit with significantly smaller amplitude than measured previously and with more variability in the locking position. Further, at the present time, no in-vessel measurements of the error field have been performed. In order to better diagnose the helical structure of error fields, locked modes, and resistive wall modes in NSTX, internal toroidal arrays of radial and vertical field sensors placed above and below the mid-plane have been installed and are presently being commissioned. Accurate relative position measurement and calibration of these sensors should allow the eventual inference of PF coil and other structural asymmetries. Importantly, these sensors are located much closer to the plasma surface to better detect the reduced amplitude locked modes and resistive wall modes. These sensors will ultimately be used by the plasma control system to generate real-time mode amplitudes and phases for use in active feedback algorithms.

Assessing the sources, amplitudes, and operational impact of static and time-varying error fields in tokamak devices can be very challenging – especially for those error fields due to vessel/coil motion. For instance, the present locked-mode detector set on NSTX routinely measures a 3-6 Gauss n=1 radial error field which is proportional to the polarity-dependent product of the TF and OH coil currents. Given these difficulties and the potential benefits of further reducing the error field, the error-field reduction techniques planned for the next five-year period will include both structural improvements/alignments where possible *and* active error-field correction/suppression. The active coils of this correction system will be comprised of six (1 meter tall and 55-60° toroidal extent) ex-vessel picture frame coils much like the DIII-D error-field correction "C-coils." These coils will be placed symmetrically around the outboard mid-plane of NSTX, centered vertically between the primary passive plates, and close to the vessel wall. These coils and their associated power supplies will be capable of generating at least 40 Gauss of n=1 radial field at the plasma surface. This capability provides a significant safety margin in the event that large previously undiagnosed error fields are discovered. It also allows a significant non-resonant n=3 field to be generated which may prove useful for toroidal rotation control. Finally, sufficiently fast power supplies will allow fast feedback of the RWM in low-rotation plasmas as described in later sections.

Error fields and locked modes — Plans

Goal: Measure, then correct non-axisymmetric error fields through engineering improvements and externally applied and controlled n=1 radial fields.

FY2003-04 Perform experiments using low-density locked modes and beam pulses to determine locking threshold as a function of density, rotation, magnetic field, and current. Use locking position to aid inference of error-field sources. Commission internal RWM/EF sensor array electronics. Gather engineering data on primary passive plate misalignment and sensor positions and calibrate signals including effects of position. Begin assessment of sources of error field such as PF coils or passive plates.

FY2004 Install active coil set. Commission TFTR Transrex and/or new Robicon Switching Power Amplifiers (SPAs). Interface supply controls to PCS. After utilizing internal sensor measurements to infer sources of error field, correct error fields directly where possible through re-alignment. Determine estimated correction coil currents for canceling residual error fields without active feedback. Perform experiments varying applied error-field to minimize rotation damping near and above no-wall limit. Compare predicted currents for optimal error-field suppression to those that minimize rotation damping. Develop PCS control algorithms to use optimal pre-programmed correction coil currents.

FY2004-05 Purchase and install data acquisition for PCS to acquire needed magnetic sensor signals in real-time for fast feedback control. Implement calibration algorithms for in-vessel RWM/EF sensor signals.

FY2005-06 Utilize real-time internal sensor measurements during plasma operations and develop dynamic error-field correction algorithms. Supplement or replace pre-programmed error-field correction with dynamic error-field correction.

FY06-future Study possibility of generating stochastic divertor boundary with non-axisymmetric coils. If promising, attempt to modify/improve edge confinement, ELMs, and power flux.

Beta limiting modes

Pressure-driven kink-ballooning modes and resistive wall modes have been previously shown to be beta limiting in NBI-heated NSTX discharges [17]. Neoclassical tearing modes have also recently been shown to be a concern for any ST operating regime that relies upon high poloidal beta and bootstrap fraction [18]. The following subsections discuss the modes typically observed to limit performance at the highest β_T and β_P values achieved following recent machine improvements.

Limiting modes in highest β_T discharges

Figure 3.1.3 shows that the present operating limit of $\beta_N \approx 6$ restricts the accessible β_P and bootstrap fraction for the highest β_T discharges at low $q^* < 2$. Such discharges also often have low central safety factor near 1 at high β. In such discharges, n=1 pressure-driven internal kink modes are computed to be ideally unstable and are observed to grow on 5 to 20ms time-scales and often exhibit saturation followed by slow amplitude decay. These large internal m/n = 1/1 modes can also lead to saturation in β, degradation in plasma rotation, and sometimes rapid disruption. An example of such behavior for two 1MA discharges with B_{T0} = 3kG which reach β_T =25% and 31% is shown in Figure 3.1.9. As seen in the figure, β_T exhibits saturation from t=225ms to 260ms in both discharges despite the previous increase in NBI heating power by a factor of 3. The highest β_T discharge in Figure 3.1.9 is unique in that the limiting mode amplitude decreases after t=260ms, allowing the stored energy to increase and ultimately reach β_P = 0.7 and β_N = 6.2 prior to undergoing an uncommonly rapid 400MA/s plasma current disruption. Insight into the structure of this limiting 1/1 has been gained

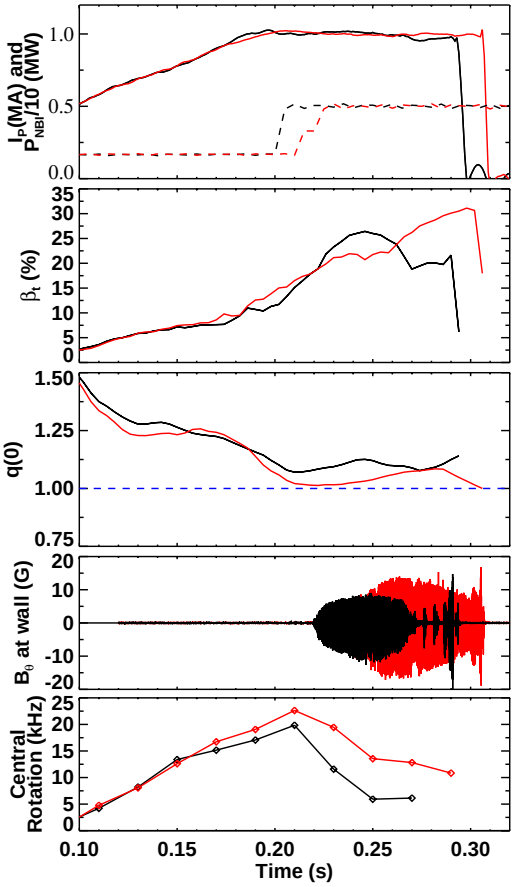

Figure 3.1.9 – Time traces of two high β_T discharges and 1/1 mode amplitudes.

by correlating the plasma rotation profiles to fluctuation spectra from the NSTX ultra-soft X-ray (USXR) array. These studies confirm that the 1/1 mode can exist at very large minor radius (up to $r/a \approx 0.6$) which likely contributes to the rapidity of the discharge termination.

Limiting modes in high β_P long-pulse discharges

In contrast to the lower β_P achievable at high β_T, Figure 3.1.10 shows time-traces of a typical high β_P=1.2 discharge with I_P=800kA, B_{T0}=4.5kG, and bootstrap current fraction of 35 to 40%. Figure 3.1.10a shows that during the first 400ms of this discharge, an n=2 mode is measured to initiate near 300ms coincident with a short burst (amplitude spike) of n=1 activity. At t=430ms, Figure 3.1.10c shows that another burst of n=1 activity causes a drop in β_P followed by a subsequent re-heat of the plasma. After this burst at 430ms, Figure 3.1.10d shows that a longer-lived lower-frequency n=1 mode initiates which may be a neoclassical tearing mode (NTM). Figure 3.1.10e shows that each continuous mode and n=1 burst event decreases the central rotation speed, and following the second collapse of β_P at t=500ms, the rotation decay is accelerated. Finally, Figure 3.1.10f shows that after the plasma rotation is below approximately 2 to 4kHz across most of the profile, the n=1 locked-mode signal increases rapidly and leads to a rapid decay in β_P prior to beam turn off at t=600ms. Clearly, understanding the origin of the bursting n=1 modes and the other continuous and long-lived modes they trigger at high β_P and β_N is an important element to further lengthening NSTX discharges and raising β_N.

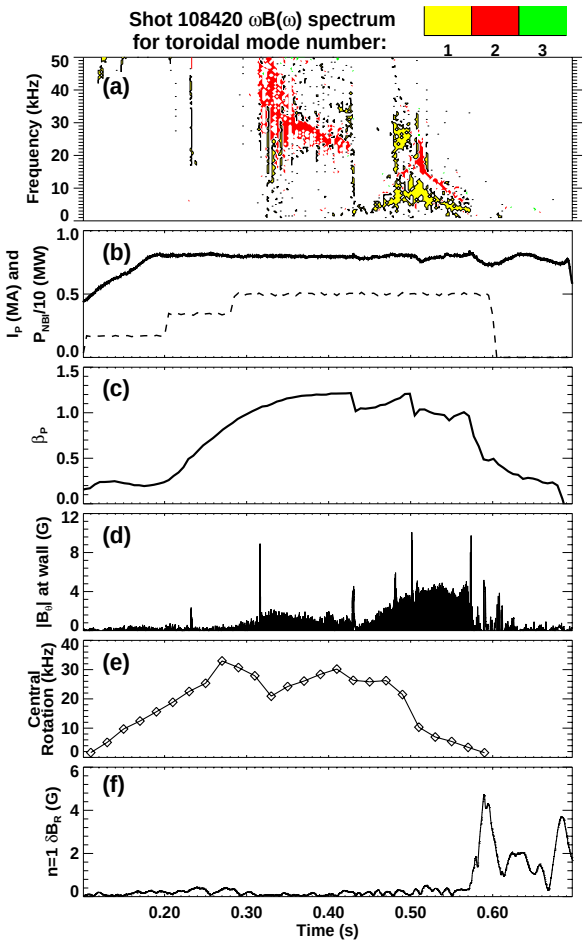

Figure 3.1.10 - Time traces of a high β_P discharge (a-c) and rotating and non-rotating (n=1) mode amplitudes (d,f).

To attempt to better understand the limiting modes observed in Figure 3.1.10 above, the time-evolution of the n=1 ideal MHD stability criteria computed with the DCON [19] code both with and without a conducting wall is shown in Figure 3.1.11 for discharge 108420. The RWM growth time as computed by the coupled DCON and VALEN [20] codes is 15 ms as β_N increases beyond the no-wall beta limit, $\beta_{Nno\text{-}wall} \approx 5$ near t= 300ms. However, as β_N reaches a peak value of over 6.1, VALEN shows a greatly decreased mode growth time of 30 μs, indicating that the with-wall beta limit, β_{Nwall}, is being approached and passive wall stabilization has become less effective. At this point, a beta collapse occurs in the plasma reducing β_N to 4.8. The ideal n=1 no-wall stability criterion computed by DCON shows this value to be close to marginal stability. The collapse occurs over a few hundred microseconds, consistent with an ideal mode being heated through the stability limit. In addition, this initial and subsequent beta collapses correlate exactly with collapses of the measured neutron rate as shown in Figure 3.1.12. Since neutron creation occurs almost exclusively in the plasma core, the collapses indicate that the mode is internal. Using the relatively large value of τ_{wall}= 15 ms for the n=1 RWM perturbation computed with DCON and VALEN when β_N initially exceeds $\beta_{Nno\text{-}wall}$, a conservative estimate of the plasma duration with $\beta_N/\beta_{Nno\text{-}wall}$ greater than unity is 18 τ_{wall}. The fast, repeated beta collapses shown in Figure

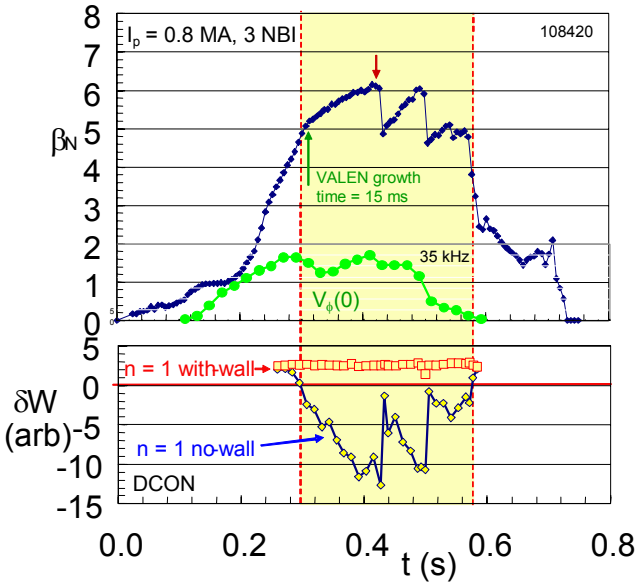

Figure 3.1.11 - Evolution of β_N , V_ϕ and ideal no-wall and with-wall stability criteria for a plasma exceeding $\beta_N/\beta_{Nno\text{-}wall}$=1.3 and approaching β_{Nwall}.

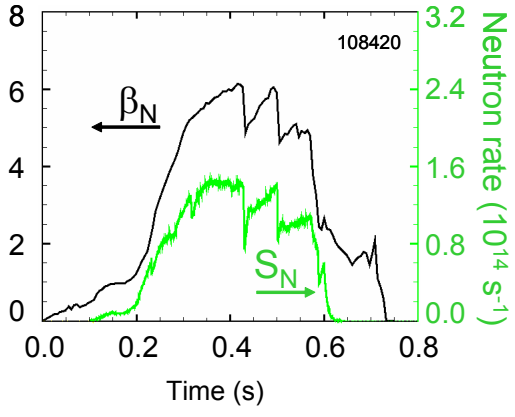

Figure 3.1.12 - Correlation of neutron rate and β_N during beta collapses in high β_N plasma.

3.1.10 are correlated with the magnitude of β_N, since similar plasmas have been maintained for longer pulse lengths (duration of greater than $20\,\tau_{wall}$) at a nearly constant value of $\beta_N = 5.6$ *without* fast beta collapses. For the discharge shown in Figure 3.1.10, DCON shows that the plasma is also unstable to the n=2 mode shortly after n=1 instability is determined. Plasma instability to multiple n values was anticipated at high β_N, and future work will investigate the presence of n=2 and possibly n=3 signatures measured by the new internal sensor arrays.

Resistive wall mode physics: rotation damping and passive stabilization — Results

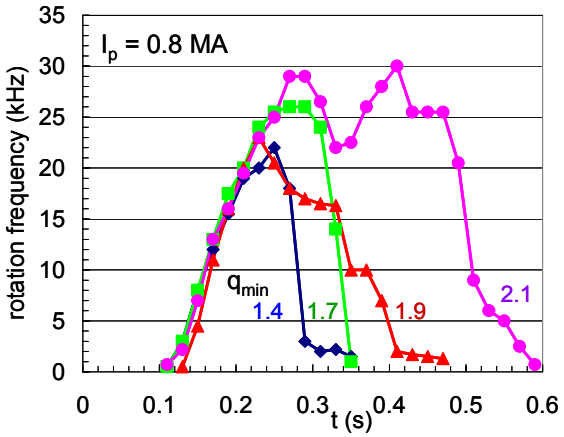

Figure 3.1.13 - Alteration of rotation evolution at constant I_p = 0.8 MA and increasing B_{T0}.

As stated above, long pulse ST plasma operation on the order of the global resistive diffusion time with $\beta_N > \beta_{Nno\text{-}wall}$ is a goal of NSTX. Since sufficient plasma rotation is required to stabilize low-n kink/ballooning modes in the absence of external feedback, rapid rotation damping associated with RWM destabilization is potentially a major impediment in reaching this goal. However, as shown in the previous section, present results have already shown significant progress in maintaining $\beta_N > \beta_{Nno\text{-}wall}$ for many resistive wall times. A key to this success has been operation with increased applied toroidal field. Figure 3.1.13 shows the evolution of the toroidal rotation frequency in the core of the plasma for several values of B_{T0}. Also shown is the EFIT computed q_{min} (without internal magnetic field measurements from MSE) for each plasma at peak β_N. RWMs are observed in the discharges with $B_{T0} = 0.34$T ($q_{min} = 1.4$) and $B_{T0} = 0.39$T ($q_{min} = 1.7$), leading to the rapid core rotation damping. However, as B_{T0} is raised to 0.44T ($q_{min} = 1.9$), the n=1 signature of the RWM is no longer apparent in the locked mode detector signal, the rotation damping rate significantly decreases, and the pulse length is extended. The fourth case shown also has $B_{T0} = 0.44$T, but has slightly different plasma cross-section (increased elongation) and the computed q_{min} rises to slightly above 2. Empirically,

systematic analysis of EFIT reconstructions finds that only plasmas with $q_{min} > 2$ have maintained high β_N for long pulse lengths of order the current relaxation time.

Recent plasmas with reduced static error field and increased β_N exhibit significantly different behavior than RWMs at lower β_N. First, it is rare to find pure RWM activity separate from tearing mode activity. This observation might be due in part to an increased difficulty in measuring the RWM field perturbation with the present locked mode detector (LMD) at the reduced static error field. LMD signals of between 0.6–1.0 G are now more typical during the RWM (see Figure 3.1.14). A common feature between RWMs at high and low β_N is the strong toroidal rotation damping observed in both in spite of increased neutral beam momentum input over lower beta plasmas. The magnitude of the rotation damping, as well as the detail of the rotation profile dynamics distinguishes the RWM from tearing mode activity and suggests a very different physical mechanism for rotation damping between the two modes. In plasmas exhibiting rotating modes alone, rotation damping is relatively weak. Figure 3.1.14b illustrates the toroidal rotation profile dynamics for a plasma initially exhibiting n=1 and 2 rotating mode activity, with n=2 largely damped approximately 60 ms after the mode onset. Magnetic pickup coils show n=1 oscillations with a frequency slowly decreasing from 8 kHz, consistent with the observed toroidal rotation frequency, F_ϕ, decrease in the region of the EFIT computed q=2 surface. The rotation damping rate at q=2 is nearly constant at -29kHz/s. The profile dynamics show the damping to be diffusive, originating near the q=2 surface, and penetrating slowly to the plasma core. Mode locking eventually occurs 0.2s later, when rotation at q=2 drops to the critical value of approximately half the initial value, $\omega_0/2$. This process is in agreement with the theory of rotation damping due to a magnetic

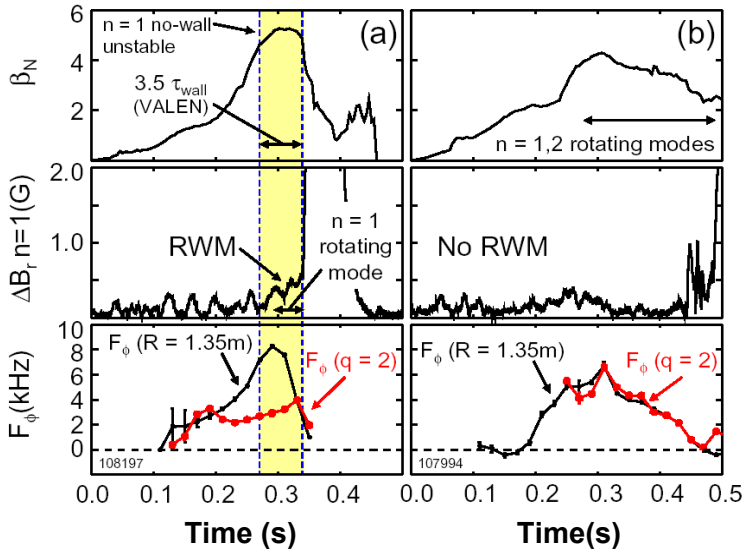

Figure 3.1.14 - Evolution of β_N, locked mode signal, and toroidal rotatio in recent NSTX plasmas above / below the no-wall beta limit.

island in the presence of a conducting wall [21]. In contrast, Figure 3.1.14a shows toroidal rotation damping occurring across most of the plasma cross-section simultaneously when the RWM is present. The process appears non-diffusive, and similar to the rotation damping process observed in error field induced locked modes when field penetration occurs [16]. The rotation damping rate near $q = 2$ in the RWM case is -174 kHz/s, six times more rapid than in the case of islands alone. It is also clear that the RWM shows only a weak signal in the locked-mode detector and is accompanied by n=1 rotating mode activity as the RWM grows. The locked- mode detector signal reaches just 0.6G before the accompanying island locks. The RWM therefore greatly reduces the time it normally takes the island to reach $\omega_0/2$. Another remarkable detail of the rotation damping process is that the edge rotation remains essentially unchanged during RWM induced rotation damping, whereas the case of slow rotation damping due to islands shows a viscous drag outside of $q = 2$. This can be qualitatively explained by invoking a model of neoclassical viscous drag in the nearly static magnetic field perturbation of the RWM [22,23]. This model has been successfully used to describe error field induced locked mode damping in JET [16]. By this physics, local rotation damping scales as $\delta B_r^2 T_i^{0.5}$, where δB_r is the local perturbed field, and T_i is the ion temperature. Therefore, it is expected that the rotation damping would be greatly reduced in the colder outer region of the plasma, consistent with the observation.

Resistive wall mode physics: rotation damping and passive stabilization — Plans

Goal: *Measure and understand flow damping from, and rotational and dissipative stabilization of, the resistive wall mode across toroidal devices.*

FY2003-04 Propose similarity experiment with DIII-D and MAST to explore (i) aspect ratio effects of these physics topics (DIII-D), and (ii) comparison of plasmas approaching and surpassing the no-wall beta limit with and without conducting structure (MAST). Perform experiments designed to investigate the nature of RWM stabilization mechanism in the presence of rotation and investigate role of the RWM itself in modifying rotation. Using MARS code, perform theoretical assessment of expected critical rotation frequency for RWM stabilization and associated scaling with safety factor, magnetic field, shape, and aspect ratio.

FY2004-05 Theoretically and experimentally determine the feasibility of operation in the "second stability region" of the resistive wall mode. Explore the existence of toroidally localized, intermediate-*n* kink/ballooning modes and associated RWMs created through error fields or tearing modes. Establish with MSE data if low *n* RWMs can be stabilized and/or rotation damping minimized through elevated q_{min} and finite rotation for high β_N operational regimes. In regimes where RWM is passively unstable above the no-wall limit, benchmark codes such as DCON+VALEN and/or MARS+VACUUM used in predicting RWM structure, growth-rate, and frequency, against measurements from the internal RWM/EF magnetic sensor set.

FY05-future Examine the role of RWMs of multiple simultaneous unstable *n* values. Using experimental results and comparison to theory, assess rotation required for stabilization of RWM in long-pulse high-β operating regimes. Use knowledge gained to test active feedback stabilization physics in regimes with low rotation speed and to project to future ST devices.

Active RWM stabilization — Motivation

While β_N values above the no-wall beta limit have been sustained for a significant number of conducting wall times in toroidally rotating NSTX plasmas at increased toroidal field, sustaining such plasmas indefinitely and at lower q^* may require fast active feedback stabilization of global MHD modes. Of particular interest for NSTX is the sustainment of high β_N when error-field correction and rotation from NBI heating are insufficient to provide rotational stabilization of the RWM, i.e. when the toroidal rotation frequency is below the critical rotation frequency for RWM destabilization. Such a system would therefore allow the study of mode stabilization under the low-rotation conditions that might be expected in an ST reactor.

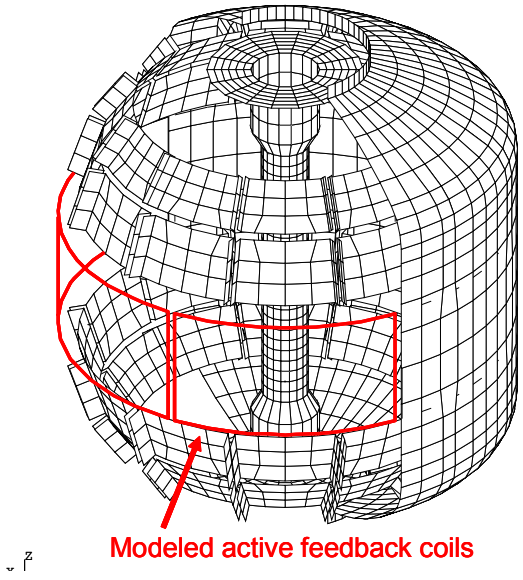

Figure 3.1.15 - Conducting structure and midplane control coil modeled in VALEN.

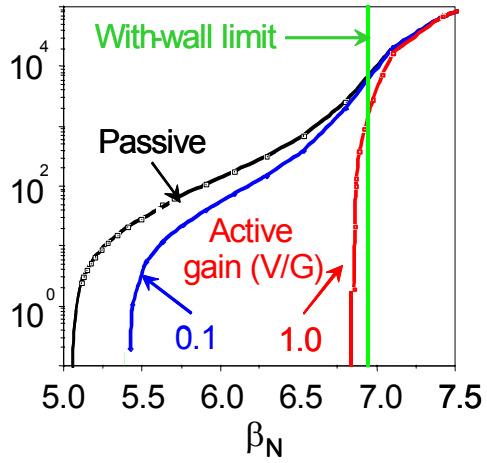

Figure 3.1.16: RWM growth rate (s^{-1}) vs. β_N as a function of gain for modeled active feedback system with internal midplane control coils.

A physics design of an active feedback system planned to be installed in NSTX has been conducted with the DCON and VALEN codes, using equilibrium input from NSTX experiments. These calculations incorporate the NSTX conducting structure designed to provide passive stabilization of the RWM. VALEN uses a finite element representation of thin shell conducting structures in an integral formulation to model arbitrary conducting walls, combined with a circuit representation of stable and unstable plasma modes. The VALEN code also has the capability to model arbitrary control coils, magnetic flux sensors, simple power supplies and control schemes that would be used to connect these items together to provide stabilization of plasma instabilities through active feedback. Previous calculations using VALEN for the DIII-D device indicate that the most effective systems have control coils positioned as close as possible to the plasma and as far away as possible from major conducting structures. A mode control scheme typically uses a global array of magnetic sensors placed inside the vacuum vessel as close as possible to the plasma and oriented to sample the poloidal field of an instability while being orthogonal to the field produced by the closest control coils. The structure of the instability may then be identified with feedback logic determining the currents or voltages applied to the control coils.

A near optimal active feedback system designed to suppress the n=1 instability in NSTX has been studied computationally. In this case, the modeled sensors are positioned inside the vacuum vessel on the plasma midplane and measure the poloidal field of the instability. As shown in Figure 3.1.15, control coils were placed inside the vacuum vessel. Six equal size picture frame coils, which produce local radial fields,

cover the mid-plane circumference of NSTX and are connected 'anti-pairwise' (control coils diametrically opposite each other are in a series circuit and their radial fields are in the same direction). The sensors have a single turn and an area of 1cm^2. The flux from the sensors is multiplied by a constant gain to determine the voltage applied to the control coils. Here, the system gain is expressed as the ratio of the control coil voltage to input field perturbation amplitude. Figure 3.1.16 illustrates the performance of this system. At a gain of 0.1 *V/G* the plasma is stable for beta normal less than 5.39. Further improvement in performance may be obtained by increasing the gain up to about 1.0 *V/G* where the plasma is stable for beta normal less than 6.83. The active feedback system shows no further improvement for additional increases in gain. Therefore, this system can stabilize the mode up to $\Delta\beta_N$ = 94% where $\Delta\beta_N \equiv \beta_N$(ideal-wall) - β_N(no-wall). Alternatives to this 'near optimal' active feedback system have also been considered, and the 'next best' system has poloidal field sensors inside the vacuum vessel, but moves the control coils outside the vacuum vessel. This system reaches a maximum stabilized $\Delta\beta_N$ = 72% — a decrease of 22% from the near optimal design. Due to considerations such as cost, system complexity and risk, implementation schedule, and the capability of performing error-field correction and RWM control with low effective supply ripple in a single system, it has been decided that this 'next-best' exterior active coil design will be the first system implemented on NSTX. This decision does not preclude the installation of a higher-performance in-vessel coil system at a later date.

Active RWM stabilization — Plans

Goal: *Design and implement an active global mode suppression system, and use it to sustain operation near the ideal wall limit.*

FY2003-04 Finalize design of active coil set using DCON+VALEN analysis. System design will include control of low-*n* modes equal to and greater than unity. System will be compatible with power/current and frequency/bandwidth requirements to simultaneously correct error fields and provide fast feedback for RWM control.

FY2004 Install active coils and power supplies (see section on error-fields for more detail).

FY2005-06 Develop techniques to control rotation speed independent of beam heating power to decouple rotation from β. Flow damping from non-resonant error-field excitation using active coils and/or controlled error-field amplification of the RWM would be possible means. In regimes where RWM is passively unstable above the no-wall limit, develop feedback algorithms to stabilize the RWM up to the ideal-wall limit. Investigate stabilization of multiple-*n* modes, possibly including toroidally localized ballooning modes. Utilize the implemented multi-*n* control coil system to create a spectrum of static *m/n* error fields to determine the effect on the RWM. Also, use non-resonant error fields to modify NTM island formation.

FY06-future Apply passive and active RWM stabilization to increase safe operating distance above no-wall stability limit in high-β long-pulse discharges. Utilize RWM feedback to sustain high β_N operation close to the ideal-wall limit in optimized long-pulse discharges.

Neoclassical tearing modes — Results

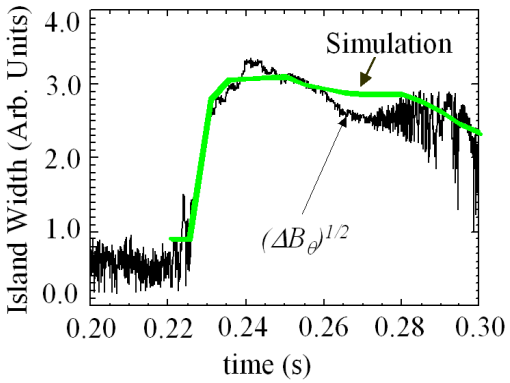

Figure 3.1.17 – Island evolution fit to a 3/2 neoclassical tearing mode in shot 104096.

Prior to error-field reduction and before routine H-mode operation, the effect of *q(0)* crossing 1 varied from mild sawtoothing (if l_i was sufficiently high) to the development of large radius *n*=1 sawteeth or kink modes (for low l_i) often resulting in locked modes that disrupted the plasma. In regimes with *q(0)* > 1, *n*=2 modes were often observed to be destabilized prior to the *m/n*=1/1 becoming unstable whenever β_P exceeded 0.4 to 0.5. This trend is evident in Figure 3.1.3 for the FY2001 data (black symbols) for discharges with *q** between 2 and 3. These *n*=2 modes had many of the characteristics of 3/2 neoclassical tearing modes including island width evolution consistent with the modified Rutherford equation. As seen in Figure 3.1.17, the island width evolution is fit reasonably well using equation parameters similar to those of standard aspect ratio tokamaks until t=260ms. At t=270ms, a 1/1 mode is measured to become unstable possibly explaining both the degraded fit just prior to 1/1 onset and the oscillations in island

width as inferred from the measured magnetic perturbation after t=270ms. At present, it is not clear if the n=2 mode in the high β_P discharge of Figure 3.1.10 is similar to the 3/2 NTM shown in Figure 3.1.17.

Neoclassical tearing modes — Plans

Goal: *Understand NTM stability physics in low aspect ratio geometry and feedback stabilize these modes if they significantly impact performance.*

FY2003-04 Implement more accurate wall shape model in PEST-III for wall-stabilized tearing mode stability studies. Implement algorithms in PEST-III to predict Mirnov signals from rotating islands, compare to experimental data, and estimate island widths.

FY2004-05 Using measured q profiles, assess seeding mechanisms for NTMs in NSTX standard and advanced operating regimes. Determine if modes are excited "spontaneously" via proximity to an ideal limit or if seeded directly from other observable MHD modes. Investigate non-linear coupling of NTMs of different helicities.

FY2005-06 Measure poloidal mode numbers magnetically utilizing improved poloidal Mirnov array. Correlate magnetically inferred m/n data to island position measurements from Soft X-ray (SXR) and possibly EBW radiometer. Infer island widths from measurements and improved modeling to assess current drive needs for EBW-CD feedback stabilization of the NTM. Perform initial NTM stabilization studies with 1 MW EBW system in 2006.

FY2006-08 Perform preliminary assessment of changes in NTM stability due to changes in current profile resulting from EBW current drive and electron heating. Assess EBW power requirements for NTM stabilization based on measurements of CD efficiency and required CD for mode stabilization. Demonstrate direct NTM suppression with pre-programmed control of launcher and plasma conditions. Verify CD requirements with NTM modeling of stabilization.

FY08-future Incorporate EBW launcher control into PCS and demonstrate active feedback stabilization/suppression of the NTM.

Edge localized modes — Results

The detailed stability characteristics of edge-localized modes (ELMs) have not yet been thoroughly investigated in NSTX. Empirically, separatrix configuration and shaping appear to play a large role in the type of ELMs observed. Most NSTX long-pulse discharges have favored lower single null operation both for easier H-mode access and for the longest durations free of large ELM activity. In contrast, double-null operation has thus far been more prone to larger ELMs disrupting long-pulse flattops. Understanding this difference is very important, as the strong shaping of highly triangular double null plasmas should enhance no-wall global stability relative to single null operation. However, ELM size also appears to be strongly related to edge fueling. Thus, edge collisionality and density effects may be complicating the interpretation of the types of ELMs observed through the edge neoclassical bootstrap current. In some modes of operation, edge MHD with some of the characteristics of an ELM can penetrate far past the pedestal region into the core plasma. This may be the result of enhanced poloidal mode coupling resulting from the enhanced toroidicity of the ST geometry. Understanding and avoiding such modes will continue to be an important element in improving long-pulse operations.

Edge localized modes — Plans

Goal: Measure and understand ELM characteristics as function of boundary shape and edge plasma conditions.

FY2003-04 Perform experiments to assess impact of divertor configuration, shaping, collisionality, and plasma-wall gaps on ELM stability properties. Characterize pedestal energy loss in various ELMing regimes and destabilization of NTMs and other modes due to ELMs.

FY2004-05 Commission very high-*n* array data acquisition for measurement of ELM toroidal mode numbers. Correlate measured mode numbers with ELM type.

FY2005-06 Use reflectometer or other high-resolution near-edge profile diagnostic to perform preliminary measurements of ELM structure.

FY06-08 Using kinetic EFITs with MSE and all available profile information, reconstruct discharges from controlled experiments designed to excite different types of ELMs. Compare ELM stability threshold, mode structure, and toroidal mode numbers to predictions from ELM stability codes such as ELITE, DCON, GATO, or PEST.

FY03-future Throughout next five-year research period, continue to develop best H-mode discharges in long-pulse discharges by balancing highest thermal confinement against tolerable ELM size and frequency.

Influence of rotation on equilibrium and stability — Results

The high rotation speed of many NSTX discharges not only impacts β limits through wall stabilization, but can also modify the underlying equilibrium itself. The centrifugal force of the spinning plasma most strongly modifies force balance near the magnetic axis where the pressure gradient would otherwise be small. An outward major-radial shift in the electron density is indeed sometimes observable as shown in Figure 3.1.18, which plots profiles of electron temperature, electron density, and thermal Alfvén Mach number M_A for an MHD-quiescent L-mode discharge heated with 1.7MW of 80keV neutral beams. For this relatively low-density discharge, approximately 2/3 of the outward centrifugal force near the axis comes from the fast-ion component. The solid line overlaying the density profile in the figure represents the gradient expected from force balance arguments and is in good agreement with the measured core gradient when the fast-ion centrifugal force is included.

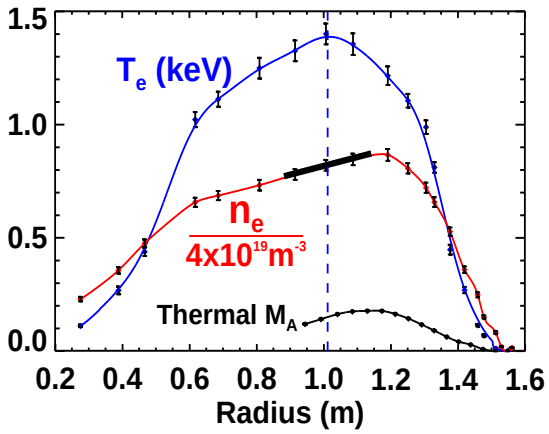

Figure 3.1.18 – Electron temperature and density showing strong in-out density asymmetry.

In addition to strong flow modifying equilibria, flow shear may also impact MHD stability. Calculations using the M3D [24] code for NSTX find that for self-consistent ideal MHD equilibria with flow included, linear growth rates of n=1 internal pressure-driven kink modes with $q(0) < 1$ can be reduced by as much as a factor of 3 due to flow-shear. Non-linearly, if sufficient shear flow is maintained and if the pressure is locally highest within the island, m/n= 1/1 mode saturation can occur. The large saturated 1/1 mode from M3D simulations shown in Figure 3.1.19 is consistent with the experimentally observed modes at high toroidal β as shown in Figure 3.1.9. This physics likely plays a role in the saturation of β and the gradual decay of the plasma rotation ultimately leading to mode locking and disruption.

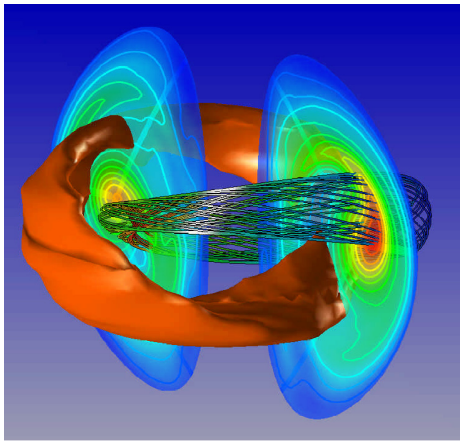

Figure 3.1.19 – Simulated contours of constant pressure (red) and island magnetic field lines (dark grey) for a saturated 1/1 mode.

Influence of rotation on equilibrium and stability — Plans

Goal: Determine the impact of thermal and fast-ion centrifugal force on core force balance and include rotation in equilibrium reconstructions and stability calculations.

FY2003-04 Assess the impact of toroidal rotation in equilibrium reconstructions. Determine change in inferred stored energy due to inclusion of centrifugal force. If effects are significant, incorporate rotation effect in control room equilibrium analysis when charge exchange recombination spectroscopy data is available. Utilize newly developed FLOW equilibrium code to include toroidal and poloidal flow and pressure anisotropy effects.

FY04-06 Use core density gradient at magnetic axis as measurement of total centrifugal force. Compare fast-ion centrifugal force to thermal, and possibly use changes in central gradient to infer changes in fast-ion population due to MHD activity. Cross check against beam-ion profile diagnostics if available, NPA, and fast-lost ion probe (FLIP). Develop stability code including flows based on FLOW equilibrium.

Fast ion induced MHD — Results

Overview

The ST in general, and NSTX in particular, is susceptible to fast-ion-driven instabilities due to the relatively low Alfvén speed compared to the neutral beam injection velocity, which is typically 2–4 times higher. Indeed, a wide variety of beam driven instabilities has been seen in NSTX at frequencies ranging from 10's of kHz to many MHz. Three beam driven instabilities commonly seen on NSTX have been identified thus far. These include: Toroidal Alfvén Eigenmodes (TAE) or Energetic Particle Modes (EPM), fishbone-type instabilities, and Compressional Alfvén Eigenmodes (CAE). In addition, less well-identified modes have also been observed. An example of a typical spectrum of MHD activity in the frequency range up to 150 kHz during NBI on NSTX is shown in Figure 3.1.20. This range includes the EPM, TAE, and fishbone, but excludes the "compressional" Alfvénic mode (CAE) activity. The first shear Alfvénic gap — the toroidal Alfvén eigenmode gap — for NSTX occurs at frequencies between about 50 and 150 kHz. These instabilities have, for the most part, an insignificant effect on fast-ion confinement or performance. One exception is during operation at reduced plasma current where bursts of TAE modes have been well correlated with abrupt neutron rate drops of order 5–10% and the expulsion of fast ions.

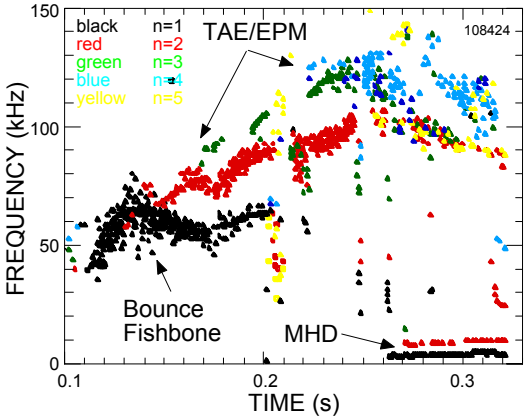

Figure 3.1.20 – Typical MHD Spectrogram for discharge with fast ion MHD.

TAE modes and fast-ion loss

The non-chirping modes in Figure 3.1.20, typically with toroidal mode number between 2 and 6, are identified as TAE modes [25]. A somewhat surprising observation is that, unlike beam driven TAE modes in conventional aspect ratio tokamaks, these modes generally seem to have a relatively small affect on the fast ion population. No obvious impact is seen on the neutron rate, nor is there an increase in the measured fast ion loss. However, in plasma conditions in which the central q is high and the beam

heating is intense, the TAE evolve from continuous modes to bursting modes, with multiple modes of different *n* present. When the multiple *n* number bursting TAE modes are present, significant fast ion losses are observed. In Figure 3.1.21 are shown waveforms of the plasma current, magnetic fluctuations as measured with a Mirnov coil, neutron rate, and D_α light. Coincident with the strong magnetic fluctuation bursts, sharp drops in the neutron rate and increases in the D_α light are seen. These observations are consistent with losses of 5–10% of the most energetic fast-ion population. In Figure 3.1.22 is shown a spectrogram of magnetic fluctuations with an overlay of symbols indicating the toroidal mode numbers. MHD bursts which are correlated with the fast-ion losses are indicated by vertical dashed lines. As can be seen, the bursts appear to consist of several modes with *n* ranging from 2 to 4.

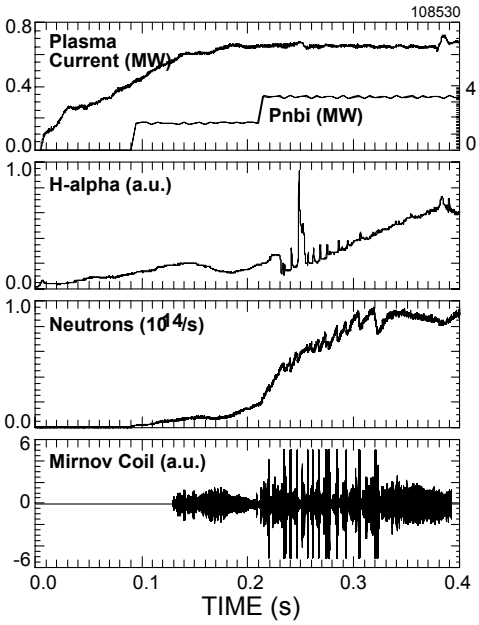

Figure 3.1.21 - Waveforms showing appearance of bursting TAE modes and fast neutron drops.

Bounce fishbone modes

The chirping modes with toroidal mode number $n = 1$ in Figure 3.1.22 are believed to be a new variant of the precession resonance fishbone [26,27] mode commonly observed in conventional aspect ratio tokamaks. The modes occur when the central q is believed to be well above unity. The fast-ion resonance condition is no longer the precession drift frequency, but at the fast-ion bounce frequency [28]. Subtracting the plasma central rotation rate, it is seen that the plasma-frame frequency of the mode chirps downward from about 45 kHz to 25 kHz. In Figure 3.1.23, this range of chirping is compared to the bounce frequencies from the ORBIT code for the fast-ion distribution calculated with TRANSP. The modes are seen to be resonant with the

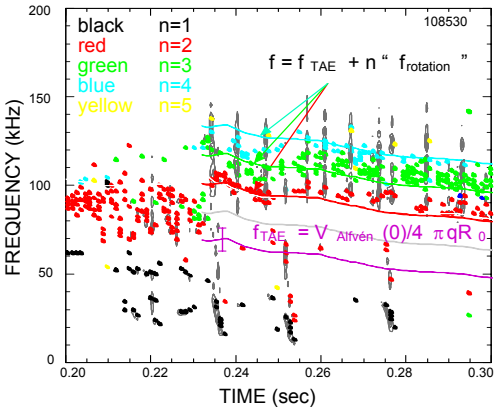

Figure 3.1.22 - Spectrogram and mode identification of TAE and other modes.

large population of beam ions with energies between 10 and 30 kV. The modes appear relatively weak; they are barely detectable in the soft X-ray emission and there is not a measurable effect on the neutron rate, implying no strong loss of fast ions. This observation of bounce-resonance fishbones has implications for conventional aspect ratio reactors in that the drift reversal expected to stabilize the fishbone instability may no longer be sufficient if the fast-ion distribution has a fast-ion population such that the average bounce angle is large, allowing resonance at the bounce frequency to drive the modes.

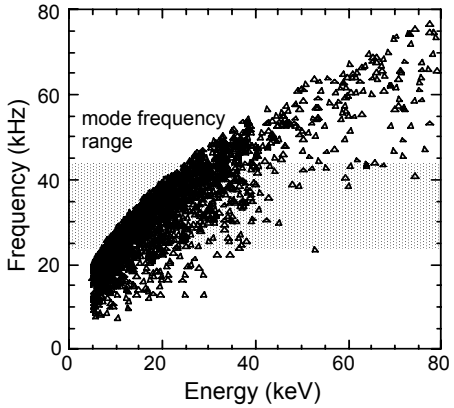

Figure 3.1.23 – Calculated distribution of fast ion bounce frequencies (ORBIT and TRANSP).

Compressional Alfvén Waves

Compressional Alfvén Eigenmodes (CAE) [29] are calculated to have a unique structure in low aspect ratio devices [30]. The strong gradient in toroidal field from the inboard to outboard plasma edge translates to a strong poloidal gradient in magnetic field strength. As a result, the modes should be localized in a "well" on the outboard edge of the plasma. The experimental observations of the CAE mode are, so far, in good agreement with the predicted mode characteristics.

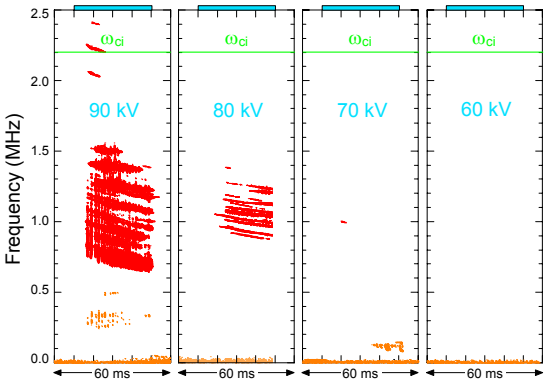

Figure 3.1.24 - Beam energy threshold for CAE.

It was also predicted that multiple CAE modes of sufficiently high amplitude could stochastically heat thermal ions [31,32]. Coupled with early measurements that suggested anomalous ion heating in NSTX, this has encouraged study of the CAE modes [33]. Experiments designed to place constraints on the fraction of beam energy available to drive the CAE instability have demonstrated that it is not likely that the *observed* CAE modes can be entirely responsible for an anomalously high ion/electron temperature ratio. As seen in Figure 3.1.24, there is a clear threshold in beam energy necessary to trigger these CAE instabilities. The threshold has a strong offset linear dependence on beam voltage and toroidal field, and

the threshold is more complicated than a simple $V_{beam} / V_{Alfvén}$ threshold. For typical NSTX parameters, the beam energy threshold is at least 55 kV. With only 66% of the beam power in the full-energy component, this means that less than ≈ 20% of the power of 80 kV beams is available to drive the CAE. As the 60-80 kV beam population is disproportionately responsible for the neutron production, a symptom of significant CAE-ion heating would be a lower than expected neutron rate and a faster decay of the neutron rate following the end of NBI, neither of which is seen.

Fast-ion MHD similarity experiments

In addition to the increased ratio of fast-ion velocity relative to the Alfvén speed in ST geometry, the strong toroidicity of the ST can also influence fast ion MHD characteristics. To better understand this physics, TAE similarity experiments have been performed on NSTX and DIII-D. In these experiments, the core Alfvén speed and fast-ion injection energy and species were matched, as was the plasma shape. Figure 3.1.25 shows that the excitation threshold is at a similar value of beam beta in both devices. The most unstable TAE modes are expected to have poloidal wavelengths approximately 6 times the fast-ion Larmor radius. For NSTX parameters, this scaling implies that NSTX should observe toroidal mode numbers roughly 2–3 times lower than in DIII-D because NSTX plasmas have a higher safety factor at fixed toroidal field due to increased toroidicity (lower aspect ratio). As seen in Figure 3.1.26, lower toroidal mode numbers are observed in NSTX — consistent with expectations.

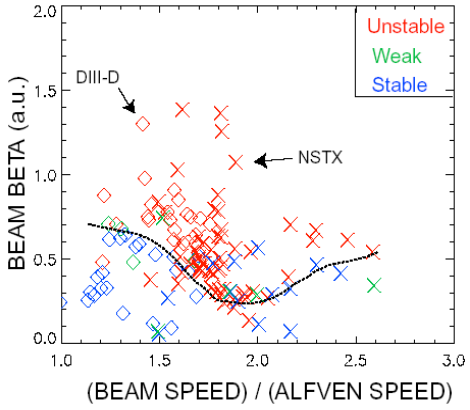

Figure 3.1.25 - comparison of TAE threshold versus beam beta in NSTX and DIII-D.

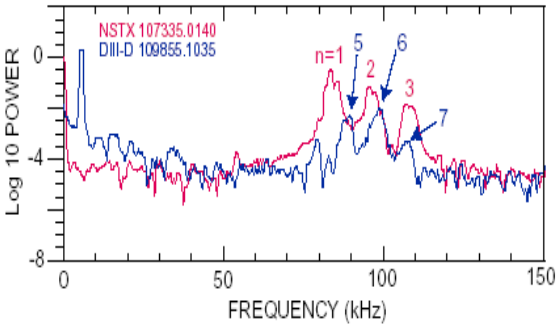

Figure 3.1.26 - Mirnov spectra for TAE modes on NSTX and DIII-D.

Fast-ion MHD — Plans

Goal: *Measure Alfvén Eigenmode stability thresholds and structure, compare to theory, and assess the impact of these modes on fast-ion confinement.*

FY2003-04 Perform similarity experiments on NSTX and DIII-D investigating the CAE to assess role of toroidicity on characteristic frequencies, stability threshold, growth rates, etc. Assess if fast ion-driven modes at low frequency such as fishbone or rTAE (f =20-40kHz) play a role in high β_P disruptions due to elevated q or destabilizing q profile (requires MSE).

FY2004-05 Perform first measurements of CAE poloidal amplitude distribution and poloidal wavelength with new outboard poloidal Mirnov array (at Bay H). Assess role of q profile in controlling gap structure for TAE modes. Correlate fast-ion loss measurements from FLIP with mode amplitude, frequency, etc. and determine the energy of ions preferentially lost.

FY2005-07 Utilize internal diagnostics including reflectometer, EBW spectrometer, or upgraded bandwidth SXR to measure internal structure of TAE, CAE, and GAE modes. Utilize fluctuation signatures and frequencies to distinguish between modes. Compare to theory and modeling with NOVA, HINST, and HYM. Assess if "pitch-angle anisotropy model" can explain drive for instabilities and thus how much energy is available to drive modes.

FY04-future Develop beam-ion profile diagnostic to determine fast-ion pressure profile. Use profile shape in ideal stability calculations and for fast-ion MHD instability drive calculations. Assess influence of fast-ion MHD on fast-ion population properties, such as neutron rate, power deposition, fast-ion angular momentum, etc. Techniques to be considered include a neutron collimator, a 3 MeV profile diagnostic, an array of active neutral particle detectors, and D-alpha light from re-neutralized beam ions.

Impact of divertor pumping and secondary passive plate modifications — Motivation

A final complicating factor in achieving high beta and bootstrap fraction for many current diffusion times in the H-mode discharges discussed above is the uncontrolled density rise in the H-mode phase. If internal disruptions and resistive wall modes can be better controlled in such scenarios with the techniques discussed above, it is expected that density limit disruptions may begin to occur unless the density saturates below the Greenwald limit. Further, having little control of the plasma density in high performance discharges makes it very difficult to assess the dependence of MHD stability on density and collisionality. The potential operational and physics capabilities offered by density control have motivated the consideration of divertor pumping by the NSTX research team. As has been experienced in several other tokamak experiments, density control through divertor pumping comes at the cost of reduced flexibility in discharge shape. Since MHD stability can be a sensitive function of plasma boundary shape and proximity of nearby conducting structure, the design of a pumped divertor will be closely tied to MHD equilibrium and stability considerations.

Impact of divertor pumping and secondary passive plate modifications — Plans

Goal: *Study and optimize the design of a divertor pumping system consistent with acceptable shape flexibility and minimal negative impact on stability.*

FY2003-04 Identify (experimentally and computationally) high-performance DND and SN discharges that are compatible with upper and/or lower divertor cryo-pumping. Use boundary and SOL geometry from these discharges to generate preliminary design for pumps and ducts. Determine passive plate modifications consistent with pump design. Calculate impact of passive plate modifications on wall stabilization of present experimental and future target discharges. Assess which plasma shapes would no longer be achievable with the modified divertor, and which shapes can be pumped.

FY2005-08 Assuming the cryo-pumps are installed, operational, and can pump: assess the impact of pumping on MHD stability. Assess changes in pressure peaking due to pumping and correlate with changes in global stability limits. Measure changes in NTM and ELM

modes with reduced core and edge collisionality. Measure changes in Alfvén Eigenmode structure and amplitude caused by lower density operation. Assess impact of changes in NBI and BS current density profiles on global, NTM, ELM, and AE stability.

3.1.4 Summary of Research Goals for FY2004-2008

The major NSTX MHD research goals by topical area from section 3.1.3 are re-stated below to summarize the proposed research plan for the upcoming five-year period. The proposed research program time line is shown following these goals.

- **Influence of profiles and shape on global stability**
  Measure and control the discharge shape and profiles to optimize stability and maximize the pulse duration at high performance.

- **Error fields and locked modes**
  Measure, then correct non-axisymmetric error fields through engineering improvements and externally applied and controlled n=1 radial fields.

- **Resistive wall mode physics: rotation damping and passive stabilization**
  Measure and understand flow damping from, and rotational and dissipative stabilization of, the resistive wall mode across toroidal devices.

- **Active RWM stabilization**
  Design and implement an active global mode suppression system, and use it to sustain operation near the ideal wall limit.

- **Neoclassical tearing modes**
  Understand NTM stability physics in low aspect ratio geometry and feedback stabilize these modes if they significantly impact performance.

- **Fast-ion MHD**
  Measure Alfvén Eigenmode stability thresholds and structure, compare to theory, and assess the impact of these modes on fast-ion confinement.

- **Edge-localized modes**

  Measure and understand ELM characteristics as function of boundary shape and edge plasma conditions.

- **Impact of divertor pumping and secondary passive plate modifications**

  Study and optimize the design of a divertor pumping system consistent with acceptable shape flexibility and minimal negative impact on stability.

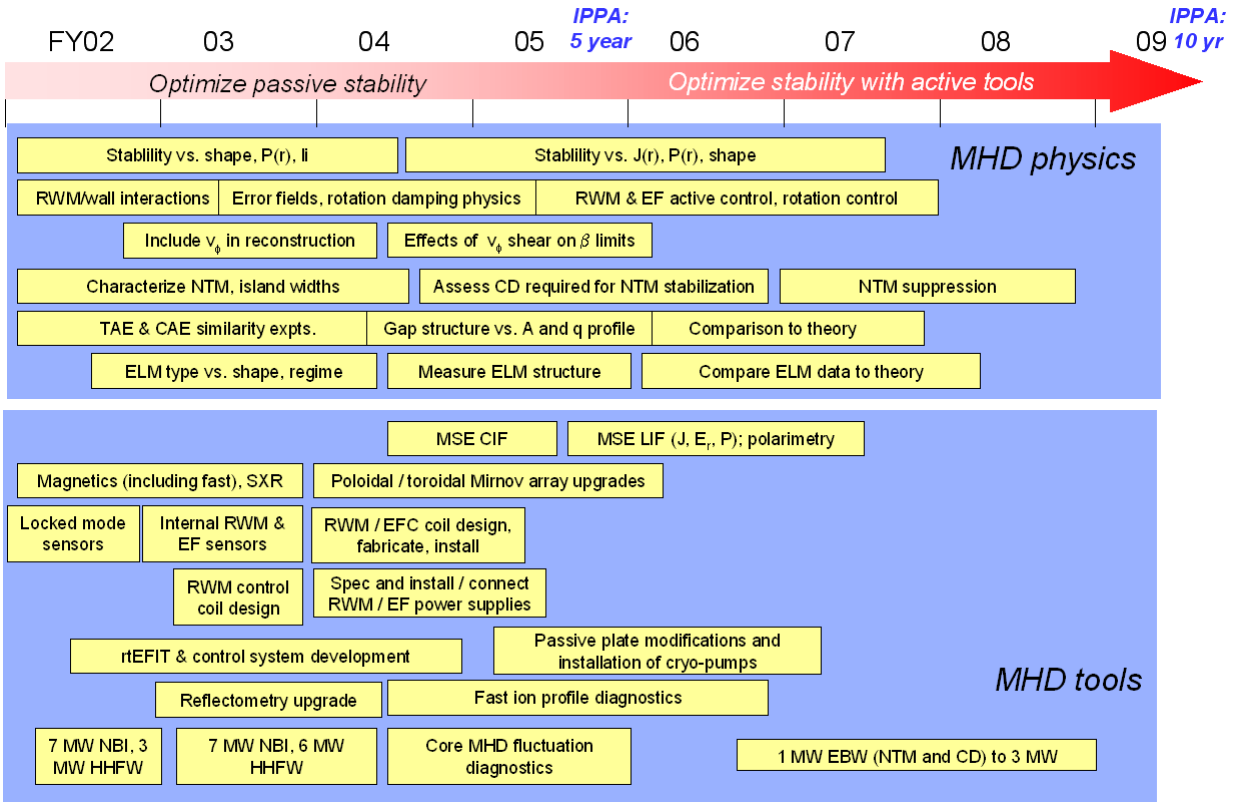

References

[1] Peng, Y.-K.M. and Strickler, D.J., Nucl. Fusion **26** (1986) 769.

[2] Howl, W. *et al.,* Phys. Fluids B **4**, (1992) 1724.

[3] Sabbagh, S.A. *et al.*, Phys. Fluids B **3**, (1991) 2277.

[4] Strait, E., Phys. Plasmas **1** (1994) 1415.

[5] Kessel, C., *et al.* Phys. Rev. Lett. **72** (1994) 1212.

[6] Turnbull, A.D. *et al.*, Phys. Rev. Lett. **74** (1995) 718.

[7] Menard, J.E. *et al.*, Nucl. Fusion **37** (1997) 595.

[8] Strait, E.J. *et al.*, Phys. Rev. Lett. **74**, (1995) 2483.

[9] Bondeson, A. and Ward, D. J., Phys. Rev. Lett. **72** (1994) 2709.

[10] Garofalo, A.M. *et al.*, Nucl. Fusion **40** (2000) 1491.

[11] Garofalo, A.M. *et al.*, Phys. Rev. Lett. **89** (2002) 235001-1.

[12] Stambaugh, R.D. *et al.*, Fusion Technology **33** (1998) 1.

[13] Maingi, R. *et al.*, Phys. Rev. Lett. **88** (2002) 035003.

[14] LaHaye, R.J. *et al.*, Phys. Fluids B **4** (1992) 2098.

[15] Hender, T. *et al.*, Nucl. Fus. **32** (1992) 2091.

[16] Lazzaro, E. *et al.*, Phys. Plasmas **9** (2002) 3906.

[17] Sabbagh, S.A. *et al.*, Phys. Plasmas **9** (2002) 2085.

[18] Buttery, R. J. *et al.,* Phys. Rev. Lett. **88** (2002) 125005.

[19] Glasser, A. and Chance, M., Bull. Am. Phys. Soc. **42** (1997) 1848.

[20] Bialek, J. *et al.,* Phys. Plasmas **8** (2001) 2170.

[21] Fitzpatrick, R., Nucl. Fusion, **7** (1993) 1049.

[22] Smolyakov, A.I. *et al.*, Phys. Plasmas **2** (1995) 1581.

[23] Shaing, K.C. *et al.*, Phys. Fluids **29** (1986) 521.

[24] Park, W. *et al.*, Phys. Plasmas **6** (1999) 1796.

[25] Gorelenkov, N.N. *et al.*, Phys. Plasmas **7** (2000) 1433.

[26] PDX Group, Princeton Plasma Physics Laboratory, Phys. Rev. Lett. **50** (1983) 891.

[27] White, R.B. *et al.*, Phys. Fluids **26** (1983) 2958.

[28] Fredrickson, E., White, R., Chen, L., (in preparation).

[29] Gorelenkov, N.N., Cheng, C.Z., Nucl. Fusion **35** (1995) 1743.

[30] Fredrickson, E.D. *et al.*, Phys Rev. Lett. **87** (2001) 145001.

[31] Chen, L., Lin, Z., and White, R.B., Phys. Plasmas **8** (2001) 4713.

[32] Gates, D., White, R., Gorelenkov, N., Phys. Rev. Lett. **87** (2001) 205003.

[33] Fredrickson, E.D. *et al.*, Phys. Plasmas **9** (2002) 2069.